IEEE Access
Multidisciplinary ⋮ Rapid Review ⋮ Open Access Journal

Received 29 November 2023, accepted 14 December 2023, date of publication 19 December 2023,
date of current version 11 January 2024.

*Digital Object Identifier 10.1109/ACCESS.2023.3344654*

RESEARCH ARTICLE

# Physical Layer Security With Near-Field Beamforming

**JOÃO FERREIRA, JOÃO GUERREIRO, (Senior Member, IEEE), AND RUI DINIS, (Senior Member, IEEE)**
Faculdade de Ciências e Tecnologia da Universidade Nova de Lisboa (FCT-UNL), 2829-516 Caparica, Portugal
Instituto de Telecomunicações, 1049-001 Lisbon, Portugal

Corresponding author: João Ferreira (jpsr.ferreira@campus.fct.unl.pt)

This work was supported by Fundação para a Ciência e a Tecnologia (FCT) and Instituto de Telecomunicações (IT) under Project CELL-LESS6G 2022.08786.PTDC and Project UIDB/50008/2020.

**ABSTRACT** Extremely large antenna arrays (ELAAs) are being proposed for sixth-generation (6G) systems as an evolution of massive multiple-input, multiple-output (mMIMO). Besides having a large number of antennas, ELAAs can be physically large, which makes communication in the radiative near-field very likely. This means the plane wave approximation does not hold and channel models that accurately capture the propagation effects in the near-field are required. Recent works have highlighted the beam-focusing effect available in the near-field region, where antenna arrays can generate beams not only limited in width but also limited in depth. This work leverages a precise channel model for ELAAs intending to explore the inherent physical layer security (PLS) features in the radiative near-field. For that purpose, it is presented a study on the power ratio between a legitimate and a malicious user, considering the effects of the field region, relative distance, and beamforming direction. By taking advantage of that analysis, it is shown that both the jamming rejection and the secrecy rate can be substantially improved when communicating in the near field, demonstrating that beam-focusing constitutes an interesting PLS technique for upcoming 6G communications.

**INDEX TERMS** Massive MIMO, extremely large antenna arrays, near-field, physical layer security, secrecy rate.

## I. INTRODUCTION

Massive MIMO (mMIMO) has been employed in fifth generation (5G) for substantial spectral efficiency enhancements [1]. The preliminary visions for 6G indicate that the importance of mMIMO will persist or even increase [2]. This is justified by the need for improved data rates, increased multiplexing capabilities, and homogeneous service in the cell [3].

It is widely known that mMIMO systems provide large spatial multiplexing capabilities thanks to their high ability to filter signals in the spatial domain (i.e., very high spatial selectivity). In fact, mMIMO arrays can transmit and/or receive signals with high precision in a specific direction, yielding a very narrow half-power beamwidth (HPBW) [4]. As a consequence, the array gain decreases sharply outside the receive/transmit directions, which enables exploitation of physical layer security (PLS) features such as increased eavesdropping protection and jamming suppression [5], [6].

Secure communications are indeed one of the most important concerns in the initial sixth generation (6G) research [7], [8]. Among different PLS techniques being proposed for 6G, the use of large antenna systems is considered one of the most promising, namely by using the narrow beamforming provided by extremely large antenna arrays (ELAAs) [9].

The main difference between mMIMO and ELAAs is the higher physical size of ELAAs since both are composed of a large number of antenna elements [3]. Among ELAAs, one can distinguish between active antenna ELAAs (or surfaces), also known as large intelligent surfaces (LIS) [10], and passive ELAAs surfaces, also known as reconfigurable intelligent surfaces (RIS) [11]. Regardless of the ELAA

The associate editor coordinating the review of this manuscript and approving it for publication was Walid Al-Hussaibi.

type, their large physical size leads to a larger near-field region, being hence very likely that communications do not occur in the far-field as it is usual in conventional mMIMO. Therefore, far-field channel models based on the plane wave approximations which are used to calculate the array's response vector become inaccurate, and new channel models that accurately capture near-field effects are required [12], [13], [14].

Recently, it was shown that beamforming in the radiative near-field provides not only narrow beams but also leads to beams with finite depth [15], [16], [17]. This contrasts with the conventional, infinite-depth beamforming associated with the far-field. As an interesting consequence, ELAA can potentially focus its large gain in a particular zone, presenting a beam-focusing effect that could lead to interesting PLS features [18].

### A. RELATED WORK

PLS features of multiple-input, multiple-output (MIMO) systems have been studied in the last years. For instance, the secrecy capacity of the MIMO wiretap channel was presented in [19] and recently revisited in [20]. PLS in MIMO can be improved using several techniques, among which we have artificial noise [21], deep learning [22], power allocation [23], and other techniques (see [24] and the references therein for an overview of PLS schemes for massive MIMO with both active and passive eavesdroppers). Besides showing how MIMO systems can increase PLS, those works and the references therein use a plane wave approximation to model the legitimate and malicious MIMO propagation channels. Although we can have important PLS features due to the angular characteristics associated with the plane wave regime, especially for large antenna systems, the increasing interest in near-field communications triggered the need for appropriate channel models that take into account spherical wave propagation and all the near-field communication aspects to fully characterize the PLS features of the very large antenna arrays envisioned for 6G.

PLS benefits of near-field beamforming were first pointed out in [25]. Concretely, authors of [25] considered an extra-large (XL) multiple-input, single-output (MISO) downlink channel. They presented a PLS study concerning the achievable secrecy rate that demonstrates the benefits of near-field beamforming to achieve secure communications. In [26], the authors presented optimized hybrid beamforming algorithms for increasing the secrecy capacity in a near-field MIMO downlink channel and highlighted the security advantages of communicating in this field zone. While [25], [26] considered downlink transmissions, [27] studied the PLS features in the near-field of an ELAA for uplink communications and demonstrated that the jamming rejection can substantially increase when communication occurs in the near-field.

The main relevant work to this manuscript and their limitations are summarized in Table 1.

**TABLE 1. Main relevant work and their key limitations.**

| Ref. | PLS Aspects | Limitations |
|---|---|---|
| [19] | Secrecy rate with conventional beamforming. | Only suitable for conventional, "small" MIMO systems; Assumes far-field and plane wave approximation for channel modeling. |
| [20] | Secrecy rate with conventional beamforming. | Only valid for mMIMO; Assume far-field communications and a plane wave approximation for channel modeling. |
| [21]–[23] | Secrecy rate using artificial noise, deep learning, or power allocation, respectively. | |
| [24] | Overview of PLS for mMIMO systems. | |
| [25] | Secrecy rate with conventional beamforming. | Valid for ELAAs and near-field but consider simple uniform linear arrays (ULAs) with isotropic antenna elements and simplified downlink channel models. |
| [26] | Secrecy rate with optimized beamforming techniques. | |
| [27] | Jamming rejection with conventional beamforming. | Valid for ELAAs and near-field but only studies uplink communications. |

### B. MAJOR CONTRIBUTIONS

This work presents the PLS features of an ELAA considering near-field beamforming and both downlink and uplink communications. It is a profound extension of [27] and, contrarily to the approaches of [25] and [26], it considers a channel model with all spherical wave particularities. This channel model is based on uniform rectangular arrays (URAs) with aperture antennas and captures polarization, amplitude, and phase variations over the array. This substantially differs from the simplified spherical wave channel model of [25] and [26], where ULAs with isotropic antennas are considered and only the nonlinear phase variations over the array are taken into account. Also, differently from [25], [26], and [27], where optimized beamforming algorithms are presented, the main goal of this work is to highlight the benefits of the beam-focusing effect in PLS using propagation arguments such as the normalized antenna array gain.

The impacts of near-field beamforming in this work are presented by taking advantage of the channel model presented in [12] and [16]. The power ratio between a legitimate user and a malicious user is presented in a way that emphasizes the impact of the beamforming gain independently of the natural effect of increased PLS that naturally arises when the distance between the users increases. Subsequently, both the secrecy rate associated with downlink transmissions and the jamming rejection of uplink transmissions are presented. The main contributions of this work can be summarized as follows:

- Definition of a line of sight (LoS) channel model valid for the near-field of an ELAA that is suitable for non-broadside directions and considers all particularities of the non-plane wave regime;

- Analysis of the power ratio between a legitimate and a malicious user that decouples the impact of the relative distance between users and the ability of the ELAA to filter signals in the spatial domain;
- A study on the downlink secrecy rate considering different field regions. It is demonstrated that the secrecy rate can increase if the legitimate user is located in the near-field region, thanks to the beam-focusing effect;
- A study on the jamming suppression features of uplink communications in the near-field where it is shown that jamming can be substantially reduced with the beam-focusing effect.

For the considered scenarios, it is shown that the field region where communication takes place has a considerable impact on the PLS. This is justified by the fact that beamforming in the near-field allows for maximization of the array factor in a given zone (i.e., the beamforming gain is limited in width and depth). As a result, signal-to-noise ratio (SNR) loss of a malicious user is magnified, leading to an increase PLS. Moreover, it is shown that the fraction of active antennas of the ELAA can be adjusted according to the indented level of required protection, which constitutes an interesting PLS feature for upcoming 6G communications.

### C. ORGANIZATION & NOTATION

This work is divided into the following sections: Section II concerns the description of the adopted geometry and the considered communication scenario. Section III is dedicated to the channel modeling in the near-field. Section IV takes advantage of the channel model described in Section III and presents an analysis concerning the PLS aspects associated with ELAAs operating in different field regions. Finally, Section V presents the conclusions of this work.

#### 1) NOTATION

The notation is as follows: Boldface capital letters or symbols denote matrices. $\mathbf{X}_{ij}$ represents the element on the $i$th row and $j$th column of the matrix $\mathbf{X}$. Boldface lowercase letters represent vectors. The $n$th element of a vector is represented as $\mathbf{x}_n$. It is considered that vector representing a position in a regular rectangular coordinate system can be expanded as $\mathbf{v} = v_x\hat{\mathbf{e}}_x + v_y\hat{\mathbf{e}}_y + v_z\hat{\mathbf{e}}_z$ with $\hat{\mathbf{e}}_x$, $\hat{\mathbf{e}}_y$ and $\hat{\mathbf{e}}_z$. $||\mathbf{v}||$ denotes the norm of $\mathbf{v}$ and $\hat{\mathbf{v}} = \frac{\mathbf{v}}{||\mathbf{v}||}$ represents the direction of $\mathbf{v}$. $(\mathbf{v}\cdot\mathbf{u})$ is the dot product between $\mathbf{v}$ and $\mathbf{u}$. $(\cdot)^H$ represents the Hermitian operator (i.e., transpose conjugate). $\mathbf{I}_N$ is the $N\times N$ identity matrix. $\text{mod}(a,b)$ yields the remainder of an the integer division $\frac{b}{a}$. $\lfloor\cdot\rfloor$ is the floor function. $\mathrm{j}=\sqrt{-1}$ is the imaginary unit.

## II. SYSTEM CHARACTERIZATION

It is considered a LoS scenario where a legitimate user equipped with a single antenna communicates with an active ELAA using carrier frequency $f_c$ ($\lambda = \frac{c}{f_c}$ denotes the corresponding wavelength and $c$ is the speed of light). The ELAA is deployed in the YZ plane and is composed of $N$ edge-to-edge square aperture antennas with area $A$. The center of the $n$th antenna is defined as $\underline{p_n} = (0, y_n, z_n)$, with $y_n = -\frac{(\sqrt{N}-1)L}{2} + L \mod((n-1),\sqrt{N})$ and $z_n = \frac{(\sqrt{N}-1)L}{2} - L\lfloor\frac{n-1}{\sqrt{N}}\rfloor$, where $n = 1,\cdots,N$. The index of the center antenna of the ELAA is defined as $n_c = \frac{\sqrt{N}-1}{2}\sqrt{N} + \frac{\sqrt{N}-1}{2} + 1$. The ELAA is centered on the origin as shown in Fig. 1.

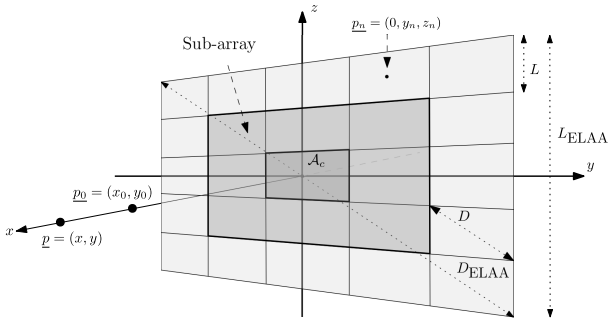


**FIGURE 1.** Considered scenario with an ELAA deployed on the YZ plane.

Each aperture antenna has side $L$, area $A = L^2$ and diagonal $D = L\sqrt{2}$. Therefore, the side of the ELAA is $L_{\text{ELAA}} = L\sqrt{N}$ and the diagonal is $D_{\text{ELAA}} = \sqrt{N}D$. The area of the ELAA is $A_{\text{ELAA}} = NA = N\frac{D^2}{2}$. It is considered the possibility of using a square sub-array inside the ELAA formed by $Q \le N$ active antennas. To characterize the dimension of this sub-array, it is defined the ELAA occupation ratio as $O = \frac{Q}{N}$.

Two users can communicate with the ELAA, one at a "reference" position $\underline{p_0}$ and another at $\underline{p}$. Without loss of generality, it is considered that both users are equipped with an isotropic antenna (i.e., point source) characterized by an effective area $A_T = \frac{\lambda^2}{4\pi}$ (which is equivalent to unitary gain $G_T = 1$) and excited with a current density directed along the $z$ axis. Unless it is otherwise stated, in the remainder of the paper it is considered an ELAA with $N = 125^2$ antennas, each with diagonal $D = 0.25\lambda$. Although this number of antennas is very large (the ELAA occupies an area of roughly $5\text{m}^2$), it is in agreement with the literature, where it has been envisioned beyond-5G use cases based on ELAAs occupying the entire facade of a building [10]. Moreover, a carrier frequency $f_c = 3$ GHz is adopted.

## III. NEAR-FIELD CHANNEL MODELLING

Modeling the underlying propagation aspects of the communication link becomes crucial when large antenna arrays are considered [14], [15], [16], [17]. This is justified by the fact that the far-field distance becomes very large, meaning that it is very likely that the communication occurs in the near-field. In fact, even if the propagation distance is larger than the so-called Fraunhofer distance ($\mathcal{D}_F$) of each antenna element, $\mathcal{D}_F = \frac{2D^2}{\lambda}$, it might be substantially lower than the Fraunhofer array distance $\mathcal{D}_{FA}$, which is $N$ times larger, i.e., $\mathcal{D}_{FA} = 2\frac{D_{\text{ELAA}}^2}{\lambda} = N\frac{2D^2}{\lambda} = N\mathcal{D}_F$.

In the near-field regime, the curvature of the impinging wave should be considered when deriving the channel model, namely through a characterization of the electric field components responsible for generating power [12]. This substantially differs from the conventional plane wave regime usually adopted in mMIMO literature, where each antenna of the array is seen as a single "point" from an electromagnetic perspective and neither the variations of effective area nor variations of polarization losses across the array are taken into account.

In the following, it is presented a channel model considering an uplink transmission (i.e., for a scenario where the legitimate user is transmitting to the ELAA). By taking advantage of the principle of reciprocity [28], this channel model will also be used for the downlink configuration.

The channel model for single antennas is presented in Subsection III-A. The channel model for ELAA with a large number of electrically small antennas is presented in Subsection III-B. The array and beamforming gains of ELAAs are characterized in Subsection III-C.

### A. SINGLE ANTENNA

Let us consider a user located at $\underline{p} = (x, y, z)$ communicating with a square aperture antenna. The user position also defines the affix of the vector $\mathbf{p} \in \mathbb{R}^{3\times 1} = x\hat{\mathbf{e}}_x + y\hat{\mathbf{e}}_y + z\hat{\mathbf{e}}_z$. Each receive point of the antenna has format $\underline{r} = (0, y_r, z_r)$, where $\underline{r}$ is the affix of the vector $\mathbf{r} = y_r\hat{\mathbf{e}}_y + z_r\hat{\mathbf{e}}_z$. The collection of all receive points forms the region spanned by the antenna, which is defined as $\mathcal{A} = \{(0, y_r, z_r) : -\frac{L}{2} \le y_r \le \frac{L}{2}, -\frac{L}{2} \le z_r \le \frac{L}{2}$. Our goal in this subsection is to derive the channel response of the LoS user-antenna link.

The electric field generated on a given location $\underline{r}$ is a function of the vector

$$\begin{aligned}\mathbf{d}(\underline{r}, \underline{p}) &= \mathbf{r} - \mathbf{p} = (x_r - x)\hat{\mathbf{e}}_x + (y_r - y)\hat{\mathbf{e}}_y + (z_r - z)\hat{\mathbf{e}}_z \\ &= x_d\hat{\mathbf{e}}_x + y_d\hat{\mathbf{e}}_y + z_d\hat{\mathbf{e}}_z, \end{aligned} \tag{1}$$

and the length of this vector represents the propagation distance between the points $\underline{p}$ and $\underline{r}$, i.e.,

$$d(\underline{r}, \underline{p}) = ||\mathbf{d}(\underline{r}, \underline{p})|| = \sqrt{x^2 + (y_r - y)^2 + (z_r - z)^2}. \tag{2}$$

The electric field structure is closely related to the vector defined in (1). More concretely, it can be computed through Green's tensor function [13]. In the following, it assumed that all points of the receive aperture are beyond the near-field of the point source ($d(\underline{r}, \underline{p}) > \lambda$), i.e, the near-field effects of the transmit antenna are neglected. This allows us to write an approximation of the $\mathbb{C}^{3\times 3}$ Green's tensor as[1]

$$\Gamma(\mathbf{d}) \approx -\frac{jZ_0 e^{-\mathrm{j}kd}}{2\lambda d}\left(\mathbf{I} - \hat{\mathbf{d}}\hat{\mathbf{d}}^H\right), \tag{3}$$

where $k = \frac{2\pi}{\lambda}$ is the wavenumber and $Z_0$ represents the free space's impedance. The electric field generated at a position $\underline{r}$ due to a point source at $\underline{p}$ is a $\mathbb{C}^{3\times 1}$ vector that depends on $\mathbf{d} = \mathbf{r} - \mathbf{p}$ and can be calculated as

$$\mathbf{E}(\mathbf{d}) = \Gamma(\mathbf{d})\mathbf{J}(\mathbf{p}) = E_x\hat{\mathbf{e}}_x + E_y\hat{\mathbf{e}}_y + E_z\hat{\mathbf{e}}_z. \tag{4}$$

Note that $\Gamma_{i,j}(\mathbf{d})$ represents the relation between a current density directed along the direction $\hat{\mathbf{e}}_i$ and the component of the electric field directed along $\hat{\mathbf{e}}_j$, where $i, j$ can be $x, y$ or $z$. Also, to decouple the impact of different excitations at the transmit antenna, one can write the Green's tensor as

$$\Gamma(\mathbf{d}) = \left[\Gamma_x(\mathbf{d})\ \Gamma_y(\mathbf{d})\ \Gamma_z(\mathbf{d})\right], \tag{5}$$

where $\Gamma_i$ is a $\mathbb{C}^{3\times 1}$ column vector that represents the impact of a current density oriented in the direction $\hat{\mathbf{e}}_i$ on the three electric field components ($E_x$, $E_y$ and $E_z$). As it is assumed that $\mathbf{J}(\mathbf{p}) = J_z\hat{\mathbf{e}}_z$, the electric field available on the aperture simplifies to

$$\mathbf{E}(\mathbf{d}) = \Gamma_z(\mathbf{d})J_z. \tag{6}$$

The received power at the aperture output has a contribution from each receive point $\underline{r}$ that is related to the normal component of the Poynting vector (i.e., only the power density component perpendicular to the aperture effectively contributes to the collected power). This "local" contribution is defined as the local channel coefficient

$$c(\mathbf{d}) = |c(\mathbf{d})|e^{-jkd}, \tag{7}$$

which is a complex quantity with a magnitude computed as

$$|c(\mathbf{d})| = \sqrt{\frac{4A_T}{Z_0^2}||\Gamma_z(\mathbf{d})||^2\left(\hat{\mathbf{d}}\cdot\hat{\mathbf{e}}_x\right)} = \frac{\sqrt{\left(x_d^2 + y_d^2\right)x_d}}{\sqrt{4\pi d^5}} \tag{8}$$

and with phase $-kd$, where $d$ given by (2).

The effective channel of the antenna is calculated by considering all contributions $c(\mathbf{d})$ over the antenna aperture, i.e.,

$$h(\mathbf{d}) = \sqrt{\frac{1}{A}}\int_{\mathcal{A}} c(\mathbf{d})d\mathbf{r}. \tag{9}$$

On the other hand, the received power can be computed as

$$P_R(\mathbf{d}) = P_T|h(\mathbf{d})|^2, \tag{10}$$

where $|h(\mathbf{d})|^2$ concentrates the path loss and the gains of the transmit and receive antennas.

### B. MULTIPLE ANTENNAS

Let us now consider an ELAA with $N$ antennas. In the following, (9) is used to define both the channel of each antenna as well as the achievable array gain. The local channel coefficient between a user located at $(x, y)$ and a receive point $(z_r, y_r)$ in the ELAA is

$$c(y_r, z_r) = \frac{\sqrt{\left(x^2 + (y_r - y)^2\right)x}}{\sqrt{4\pi}\left(x^2 + (y_r - y)^2 + z_r^2\right)^{\frac{5}{4}}}e^{-\mathrm{j}kd}, \tag{11}$$

which results from applying (9) to the particular geometry of Fig. 1.

[1] For the sake of notation simplicity, the dependence of $d(\underline{r}, \underline{p})$ and $\mathbf{d}(\underline{r}, \underline{p})$ with $\underline{r}$ and $\underline{p}$ are neglected and these symbols are referred as $d$ and $\mathbf{d}$, respectively.

The channel response between a user located at $(x, y)$ and the $n$th antenna of the ELAA (which spans the region $\mathcal{A}_n = \{(y_r, z_r) : y_n - \frac{L}{2} \leq z_r \leq y_n + \frac{L}{2}, z_n - \frac{L}{2} \leq z_r \leq z_n + \frac{L}{2}\}$) can be computed as

$$h_n(x, y) = \sqrt{\frac{1}{A}} \int_{\mathcal{A}_n} c(y_r, z_r)\, dy_r dz_r. \quad (12)$$

The $\mathbb{C}^{N\times 1}$ column vector $\mathbf{h}(x, y) = [h_1(x, y)\ h_2(x, y)\ \ldots\ h_N(x, y)]^T$ represents the channel responses between the ELAA and a user located at $(x, y)$, where $h_n(x, y)$ is computed as in (12).

### C. ARRAY GAIN AND BEAMFORMING GAIN

In the so-called plane wave regime, the maximum array gain of the ELAA is $G^{\text{FF}} = \frac{4\pi}{\lambda^2} A_{\text{ELAA}}$. This gain can be achieved when the communication takes place in the broadside direction and beyond the Fraunhofer array distance $\mathcal{D}_{FA}$. In that scenario, the received power can be easily estimated by the well-known Friis' formula [29]

$$P_R^{\text{FF}} = P_T \left(\frac{\lambda}{4\pi d}\right)^2 G^{\text{FF}} = P_T \frac{A_{\text{ELAA}}}{4\pi d^2}, \quad (13)$$

where $d$ is the propagation distance between the user and the center of the ELAA (i.e., the origin of the adopted coordinate system). Note that this equation predicts a received power that can increase indefinitely as long as the area of the ELAA increases, which clearly reveals the limitations of the plane wave regime. Alternatively, to capture the near-field effects, the array gain be computed as [31]

$$G(x, y) = \frac{4\pi}{\lambda^2} \frac{\sum_{n=1}^{N} \left| \int_{\mathcal{A}_n} c(y_r, z_r) dy_r dz_r \right|^2}{\int_{\mathcal{A}_{n_c}} |c(y_r, z_r)|^2 dy_r dz_r}, \quad (14)$$

where $\mathcal{A}_{n_c} = \{(0, y_r, z_r) : -\frac{L}{2} \leq y_r \leq \frac{L}{2}, -\frac{L}{2} \leq z_r \leq \frac{L}{2}\}$ is the region occupied by the center antenna. Provided that the channel responses are known, the gain in (14) can be obtained with matched filtering (MF) beamforming. In that case, the received power at the ELAA due to a signal transmitted by an isotropic source at $(x, y)$ is

$$P_R(x, y) = P_T \left( \sum_{n=1}^{N} |h_n(x, y)|^2 \right) = P_T ||\mathbf{h}(x, y)||^2. \quad (15)$$

Moreover, the received power can also be approximated by a "modified" Friis equation where the conventional far-field array gain is substituted by the one computed in (14), leading to

$$P_R(x, y) \approx P_T \left(\frac{\lambda}{4\pi d}\right)^2 G(x, y), \quad (16)$$

with $G(x, y) \leq G^{\text{FF}}$. Note also that this approximation is based on the so-called Fresnel approximation, where amplitude variations of the local channel coefficient (see (11)) over each antenna are neglected [16].

## IV. ANALYSIS OF PLS IN THE NEAR-FIELD

In the far field, channels of antenna arrays are modeled by complex values with the same magnitude with phase differences determined by the array response vector. This vector only depends on the direction-of-arrival (DoA) and on the distance between the antenna elements. As a consequence, in LoS scenarios, conventional DoA beamforming can be used to maximize the array gain in a given direction. However, as noted in Section III, if the communication takes place in the near-field, the different channels associated with the antennas of the ELAA do not have the same amplitude. Moreover, the channel phases are not characterized by simple functions of the DoA. Therefore, MF beamforming design should account for the spherical wave curvature, which therefore involves a given target position rather than a given target DoA.

In this section, the channel model introduced in Section III is used to study the inherent PLS features of ELAAs operating in different field regions. In subsection IV-A, a study on the power ratio between two users is presented, namely by considering the array gain defined in subsection III-C. This power ratio decouples the effects of the relative distance between users and the spatial selectivity of the ELAA. By taking advantage of that power ratio, the impact of communicating in different field regions on conventional PLS metrics is studied. More concretely, the secrecy rate associated with downlink communications is analyzed in subsection IV-B) and the jamming rejection associated with uplink communications is studied in subsection IV-C.

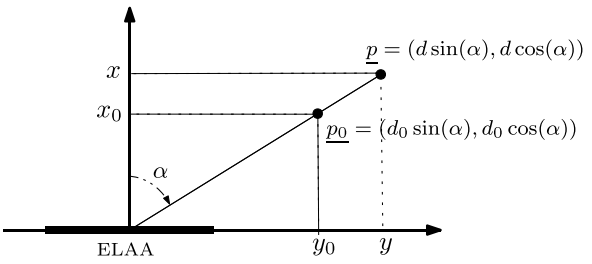


**FIGURE 2.** Top view of the considered communication scenario.

### A. POWER RATIO BETWEEN USERS

When studying classical PLS features based on the relative SNRs between users, more important than analyzing the achievable gain of a legitimate user is to evaluate the ratio between the received powers from a legitimate and a malicious user. To this end, let us start by considering the communication scenario of Fig. 2 and by defining the position of the legitimate and malicious users.[2,3] It is considered that $\underline{p_0}$ represents the legitimate user position,

[2]Since both users are located in the XY plane (i.e., $z_l = z_m = 0$), the $z$ axis coordinate is not considered for defining their locations.

[3]In what follows, it is assumed that the position of the legitimate user is perfectly known. This is supported by the strong positioning features of ELAAs [32].

i.e., the "reference" position which is the target of the beamforming. This reference position is defined as $\underline{p_0} = (x_0, y_0) = (d_0\cos(\alpha), d_0\sin(\alpha))$, with $d_0$ denoting the distance between the legitimate user and the center of the ELAA and $\alpha$ the direction of that user measured relatively to the array's broadside. On the other hand, a general position in that direction $\alpha$ that represents a potential position of the malicious user is defined as $\underline{p} = (x, y) = (d\cos(\alpha), d\sin(\alpha))$, with $d = d_0 + \Delta d$, $x = x_0 + \Delta x$, $y = y_0 + \Delta y$, where $\Delta x$ and $\Delta y$ denote the deviations relatively to $\underline{p_0}$ in the $x$ and $y$ directions, respectively. Since it is assumed that both users are in the same direction, the displacements in the $x$ and $y$ directions can be written $\Delta x = \Delta d\cos(\alpha)$ and $\Delta y = \Delta d\sin(\alpha)$.

Let us now consider the power ratio between users at $\underline{p_0}$ and $\underline{p}$. For a generic position $(x, y)$ the beamforming weights of MF are defined as

$$\mathbf{w}(x, y) = \hat{\mathbf{h}} = \frac{\mathbf{h}(x, y)}{||\mathbf{h}(x, y)||}, \tag{17}$$

which assures $||\mathbf{w}||^2 = 1$. Note that since in the considered scenario the beamforming is always designed for the "reference" position $\underline{p_0} = (x_0, y_0)$, the beamforming weights are written as

$$\mathbf{w}_0 \triangleq \mathbf{w}(x_0, y_0). \tag{18}$$

Let us now define the ratio between the power associated with a user in a generic position and the power at the reference location as

$$\begin{aligned}\bar{\kappa}(x_0, y_0, \Delta x, \Delta y) &= \frac{P_R(x_0 + \Delta x, y_0 + \Delta y)}{P_R(x_0, y_0)} \\ &= \frac{||\mathbf{w}_0^H \mathbf{h}(x_0 + \Delta x, y_0 + \Delta y)||^2}{||\mathbf{h}(x_0, y_0)||^2}.\end{aligned} \tag{19}$$

Note that by considering the alternative definition of the received power of (16), one can rewrite (19) as

$$\bar{\kappa}(x_0, y_0, \Delta x, \Delta y) = \frac{\left(\frac{\lambda}{4\pi d}\right)^2}{\left(\frac{\lambda}{4\pi d_0}\right)^2}\bar{G}(x_0, y_0, \Delta x, \Delta y), \tag{20}$$

where

$$\bar{G}(x_0, y_0, \Delta x, \Delta y) = \frac{G(x_0 + \Delta x, y_0 + \Delta y)}{G(x_0, y_0)}, \tag{21}$$

represents the normalized beamforming gain, which is defined as the ratio between array gains obtained at a general position $(x, y)$ and at the reference beamforming position $(x_0, y_0)$.

It should be highlighted that to analyze the impact of the near-field beamforming and to analyze the potential PLS features of this field region when comparing to the far-field, it is more adequate to consider that users are in the same direction. This is explained by the fact that antenna arrays can efficiently filter out signals that are coming from different directions but are not able to do it when signals are coming from the same direction, which is therefore a challenging scenario. Under these conditions the positions of both users $\underline{p_0}$ and $\underline{p}$ can be defined through the reference distance $d_0$, the displacement $\Delta d$, and direction $\alpha$. Therefore, one can rewrite the power ratio in (19) as

$$\bar{\kappa}(d_0, \Delta d, \alpha) = \frac{d_0^2}{(d_0 + \Delta d)^2}\bar{G}(d_0, \Delta d, \alpha). \tag{22}$$

Fig. 3 presents the evolution of the normalized beamforming gain in the XY plane considering users at the broadside direction, i.e., $\bar{G}(d_0, \Delta d, 0)$, fixed displacements $\Delta x$ and $\Delta y$, and two distinct reference distances: a) near-field ($d_0 = \frac{\mathcal{D}_{FA}}{30}$) and (b) far-field with ($d_0 = \mathcal{D}_{FA}$).

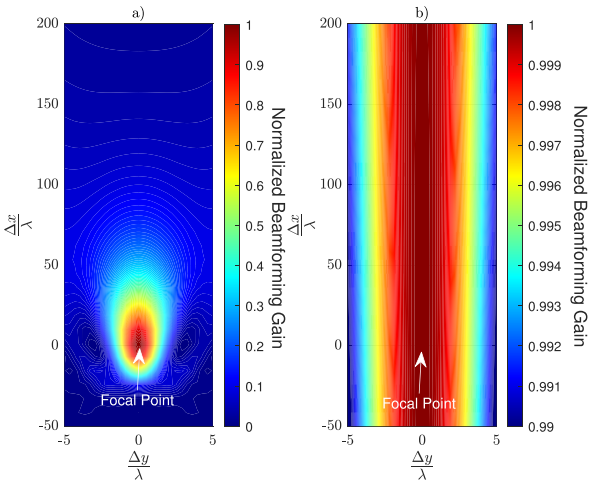


**FIGURE 3.** Normalized beamforming gain in the XY plane for the broadside direction considering two field regions: near-field with $d_0 = \frac{\mathcal{D}_{FA}}{30}$ (left figure); far-field with $d_0 = \mathcal{D}_{FA}$ (right figure).

As expected, in the far-field region (Fig. 3b)), it can be noted that the normalized beamforming gain has an infinite depth along the beamforming direction, i.e., $\bar{G}(d_0 \geq \mathcal{D}_{FA}, \Delta d, 0) = 1$, regardless of $\Delta d$. This is explained by the fact that users in the same direction experience the same array gain. Under these conditions, the ratio between received powers of (19) becomes

$$\bar{\kappa}(d_0 \geq \mathcal{D}_{FA}, \Delta d, 0) = \bar{\kappa}^{\text{FF}}(d_0, \Delta d) = \frac{d_0^2}{(d_0 + \Delta d)^2}. \tag{23}$$

As expected, in the far-field, the power ratio $\bar{\kappa}$ between users in the same direction is dominated by their relative distance, and its behavior is intuitive: for a fixed reference distance $d_0$, it naturally reduces $\Delta d$ increases. As a result, it can be noted that in this field region, the beamforming is not bringing any additional PLS feature as the ELAA is not able to spatially distinguish both users. On the other hand, the situation is different in the near-field (Fig. 3a)), where it can be that the normalized gain is concentrated around the target position. As a consequence, beamforming in the near-field (i.e., when $d_0 < \mathcal{D}_{FA}$) effectively creates a beam-focusing effect. As a result, the term $\bar{G}(d_0, \Delta d, 0)$ substantially reduces when $\Delta d$ increases, therefore it "magnifies" the SNR loss of a

malicious user relative to the target position, even if that malicious user is in the beamforming direction.

It is also interesting to study how this beam-focusing effect manifests when the ELAA is beamforming for non-broadside directions (i.e., for $\alpha \neq 0$) and in the near-field. This can be observed in Fig. 4, which shows the evolution of $\bar{G}(d_0, \Delta d, \alpha)$ in the plane XY considering a reference distance $d_0 = \mathcal{D}_{FA}/30$, different beamforming directions $\alpha$.

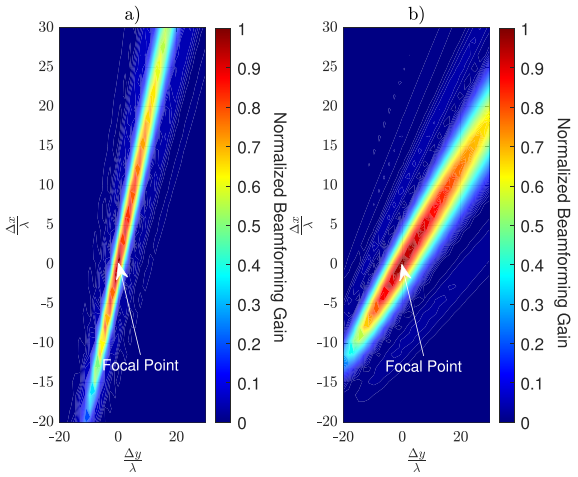


**FIGURE 4.** Evolution of the normalized beamforming gain in the plane XY considering the near-field ($d_0 = \mathcal{D}_{FA}/30$) and different beamforming directions: $\alpha = 60°$ (left figure); $\alpha = 30°$ (right figure).

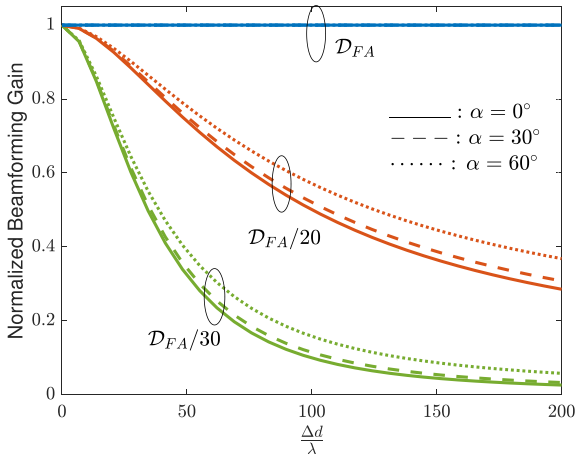


**FIGURE 5.** Evolution of the normalized beamforming along the beamforming direction considering different field regions and different beamforming directions.

From the figure, it can be noted although the beam depth is not equal for the two scenarios, the normalized beamforming gain $\bar{G}(d_0, \Delta d, \alpha)$ reduces substantially with $\Delta d$, meaning that the beam-focusing effect is available for non-broadside directions.

To further study the beam depth in the beamforming direction it is presented Fig. 5, which shows the evolution of the normalized beamforming gain considering a fixed displacement $\Delta d = [0, 200\lambda]$, different reference distances $d_0$, and different beamforming directions $\alpha$.

From the figure, it can be observed that in the far field, the normalized beamforming gain is always unitary regardless of the beamforming direction, confirming that in this field region, the power ratio between users in the same direction only depends on the relative distance between them. On the contrary, for the two other reference distances ($d_0 = \mathcal{D}_{FA}/20$ and $d_0 = \mathcal{D}_{FA}/30$) the normalized beamforming gain decreases substantially with $\Delta d$. In those scenarios, the larger the beamforming direction $\alpha$, the larger the depth of the beam. However, the impact on the focusing effect is almost negligible.

### B. SECRECY RATE

Let us consider a downlink communication scenario where the malicious user acts as an eavesdropper that tries to tap the communication link between the legitimate user and the ELAA. It is assumed that the ELAA transmits a signal with power $P_T$ that is received by both users.

It is assumed that the ELAA is precoding the signal considering MF beamforming towards a legitimate user. According to (15) and defining the beamforming weights as $\mathbf{w}_0$, the legitimate user located at $\underline{p_0} = (x_0, y_0)$ receives the signal

$$y_0 = \sqrt{P_T}\mathbf{w}_0\mathbf{h}(x_0, y_0)s + n, \tag{24}$$

where $n \sim \mathcal{CN}(0, \sigma^2)$ is the additive white Gaussian noise (AWGN) term with power $P_N = \sigma^2$. On the other hand, the received signal at a potential eavesdropper located at $\underline{p} = (x, y)$ is given as

$$y = \mathbf{w}_0^H\mathbf{h}(x, y)s + n. \tag{25}$$

Therefore, the powers of received signals of the legitimate and eavesdropper are $P_R(x_0, y_0) = P_T||\mathbf{h}(x_0, y_0)||^2$ and $P_R(x, y) = P_T||\mathbf{w}_0^H\mathbf{h}(x, y)||^2$, respectively. Together with the noise power $P_N$, which is assumed to be equal at both receiving users, these powers dictate the SNR, which can be calculated for a given position as

$$\rho(x, y) = \frac{P_R(x, y)}{P_N}. \tag{26}$$

It is widely known that channel capacity associated with a given user can be calculated as a function of its SNR [33]. More specifically, the capacity associated to a user at $(x, y)$ is

$$C(x, y) = \log_2(1 + \rho(x, y)). \tag{27}$$

The channel capacity of the legitimate user is defined as $C_0 \triangleq C(x_0, y_0) = \log_2(1 + \rho(x_0, y_0))$.

The eavesdropper's ability to tap the legitimate link is usually measured by the secrecy rate, which is computed as the difference between the capacity of the legitimate user and the eavesdropper [34], i.e.,

$$\begin{aligned} S(x_0, y_0, \Delta x, \Delta y) &= C(x_0, y_0) - C(x, y) \\ &= \log_2(1 + \rho(x_0, y_0)) - \log_2(1 + \rho(x, y)) \end{aligned}$$

$$= \log_2\left(\frac{1+\frac{1}{\rho(x_0,y_0)}}{\frac{\rho(x,y)}{\rho(x_0,y_0)}+\frac{1}{\rho(x_0,y_0)}}\right). \quad (28)$$

The secrecy rate depends on the power ratio between the legitimate user and the eavesdropper $\bar{\kappa} = \rho(x,y)/\rho(x_0,y_0)$. Therefore, by considering (19) and by assuming that both users are positioned in the beamforming direction, one can rewrite the secrecy rate as

$$S(d_0, \Delta d, \alpha) = \log_2\left(\frac{\mathrm{SNR}_0^{-1}+1}{\mathrm{SNR}_0^{-1}+\bar{\kappa}(d_0,\Delta d,\alpha)}\right), \quad (29)$$

where $\mathrm{SNR}_0^{-1} = 1/\rho(x_0,y_0)$ is the inverse of the SNR of the legitimate user.

In terms of PLS, the best scenario exists when $\bar{\kappa} \to 0$ which corresponds to a scenario where the eavesdropper is not able to receive the transmitted signal and $S \to C_0$. On the other hand, the worst scenario is when the eavesdropper has the same ability to receive the transmitted signal as the legitimate user, which traduces in a null secrecy rate (i.e., $S = 0$ bps/Hz). This only happens when both users are co-located (i.e., $\Delta d = 0$), regardless of the field region dictated by $d_0$, since $\bar{\kappa}(d_0, 0, \alpha) = 1$. For any other eavesdropper's location, $\bar{\kappa}(d_0, \Delta d, \alpha) < 1$ and a positive secrecy rate $S > 0$ bps/Hz is expected. For the same eavesdropper displacement $\Delta d$, the analysis of subsection IV-A indicates that the field region dictates how the array contributes to the PLS. As previously noted in (22), the impact of the normalized gain $\bar{G}$ on the power ratio $\bar{\kappa}$ is clearly affected by the operating field region associated with the legitimate user reference distance $d_0$, which solely relies on the relation between $d_0$ and $\mathcal{D}_{FA}$ (see Fig. 3). This means that the field region of a given user at a distance $d_0$ can be changed by modifying Fraunhofer's array distance $\mathcal{D}_{FA}$, which can be done by activating or deactivating antenna elements. As described in Section II, this scenario is modeled by considering that the ELAA can operate with a variable occupation ratio $O$.

Let us now consider an ELAA transmitting to a fixed reference location $p_0 = (x_0, y_0)$ in the broadside direction ($\alpha = 0$). This point corresponds to a reference distance $d_0 = \mathcal{D}_{FA}$ when the ELAA is operating with an occupation ratio $O = 4\%$. Fig. 6 shows the evolution of the secrecy rate considering different occupation ratios and potential eavesdropper displacements $\Delta d = [0, 1000\lambda]$ in the beamforming direction. The transmit power $P_T$ is defined to assure that the channel capacity of the legitimate user is $C_0 = 3$ bps/Hz.

From the figure, it can be noted that for small values of $\Delta d$ and regardless of $O$, the secrecy rate is very low, which is explained by the fact that both users experience the same power gain. However, as expected, as $\Delta d$ increases, the secrecy rate increases. Also, it can be observed that for a fixed value of $\Delta d$, the secrecy rate increases as $O$ increases. For instance, when the eavesdropper is at $\Delta d = 500\lambda$ from the beamforming target, the secrecy rate increases from $S = 1.6$ bps/Hz to $S = 2.2$ bps/Hz when the occupation ratio

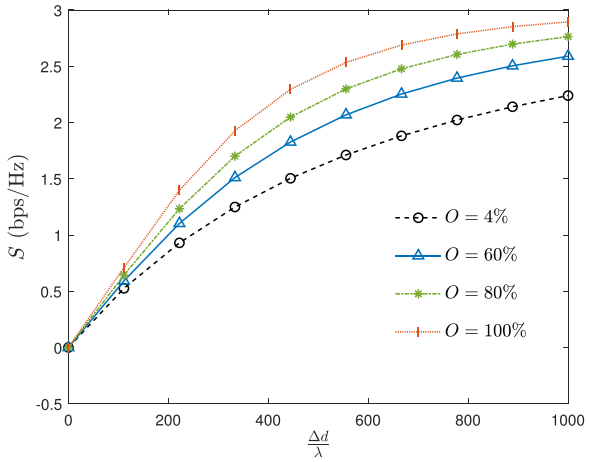


**FIGURE 6.** Secrecy rate considering an ELAA with different occupation ratios.

increases from $O = 4\%$ to $O = 80\%$. This behavior can be explained by the fact that the physical size of the sub-array effectively used for communication increases, which means that the focal point $(x_0, y_0)$ enters progressively in the near-field as $O$ increases. As a consequence, the beamforming gain imposes a reduction in the SNR of the eavesdropper. For instance, when $O = 100\%$, the reference distance is $d_0 = \frac{\mathcal{D}_{FA}}{30}$, where the beam focusing effect is available and the SNR of the eavesdropper is substantially degraded, leading to an increase in the secrecy rate. Note that since the complexity of the signal processing tasks is conditioned on the number of antennas, the ELAA might operate with an occupation ratio $O < 100\%$ (i.e., without all antennas being active) most of the time. However, when a secure downlink transmission is required, the occupation ratio can increase to force the operation in the near-field regime so that the beam-focusing effect can be exploited. This can be very useful when the security level of the communication should be increased, such as in scenarios involving key exchange processes or when very sensitive information is transmitted. This suggests that one can change the occupation ratio $O$ to manage the secrecy rate, which yields an additional degree of freedom in terms of PLS.

### C. JAMMING REJECTION

Let us now consider the uplink scenario for analyzing the jamming rejection features of the ELAA. In this scenario, it is considered a malicious user transmitting a jamming signal to sabotage the communication between the legitimate user and the ELAA. The jamming user transmits a signal with power $P_T = \beta P_T$, where $P_T$ is the power of the signal transmitted by the legitimate user and $\beta \geq 1$ is a scale factor representing the power advantage of the jamming user.

The received signal at the ELAA is composed of the sum of the signal transmitted by the legitimate user, the jamming signal, and the noise, i.e.,

$$\mathbf{y} = \mathbf{h}(x_0, y_0)s_0 + \sqrt{\beta}\mathbf{h}(x,y)s + \boldsymbol{\nu}, \quad (30)$$

where $\boldsymbol{\nu} \sim \mathcal{CN}(0, \sigma^2 \mathbf{I}_N)$ is a vector representing the AWGN components of the different receive antennas and $s_0 \in \mathbb{C}$ and $s \in \mathbb{C}$ are data symbols transmitted by the legitimate and malicious user, respectively. The ELAA employs MF combining with weights $\mathbf{w}_0$ leading to a combined signal after beamforming given by

$$\begin{aligned} \mathbf{z} &= \mathbf{w}_0^H \left( \mathbf{h}(x_0, y_0) s_0 + \sqrt{\beta} \mathbf{h}(x, y) s + \boldsymbol{\nu} \right) \\ &= \mathbf{w}_0^H \mathbf{h}(x_0, y_0) s_0 + \sqrt{\beta} \mathbf{w}_0^H \mathbf{h}(x, y) s + \mathbf{w}_0^H \boldsymbol{\nu}, \end{aligned} \tag{31}$$

where the term $\mathbf{w}_0^H \boldsymbol{\nu}$ is the combined noise with power $P_N = \sigma^2$. Therefore, the "transmit" SNR associated to the legitimate user is defined as $\text{SNR} = \frac{P_T}{P_N}$. Clearly, in the presence of a jamming signal, the capacity becomes dependent on the signal-to-noise plus jamming ratio (SNJR), which is defined as

$$\begin{aligned} \text{SNJR}(x_0, y_0, \Delta x, \Delta y, \beta) &= \frac{P_T ||\mathbf{h}(x_0, y_0)||^2}{\beta P_T ||\mathbf{w}_0^H \mathbf{h}(x, y)||^2 + P_N} \\ &= \frac{\text{SNR} ||\mathbf{h}(x_0, y_0)||^2}{1 + \beta \text{SNR} ||\mathbf{w}_0^H \mathbf{h}(x, y)||^2}. \end{aligned} \tag{32}$$

By taking advantage of (19) and by considering that both users are in the same beamforming direction, one can also write the SNJR as a function of the power ratio $\bar{\kappa}(d_0, \Delta d, \alpha)$, namely

$$\text{SNJR}(d_0, \Delta d, \alpha, \beta) = \frac{\text{SNR}}{\frac{1}{||\mathbf{h}(d_0, \alpha)||^2} + \beta \text{SNR} \bar{\kappa}(d_0, \Delta d, \alpha)} \tag{33}$$

Moreover, by defining the SNR for the legitimate user after MF as $\text{SNR}(d_0, \alpha) = \text{SNR} ||\mathbf{h}(d_0, \alpha)||^2$, it results

$$\text{SNJR}(d_0, \Delta d, \alpha, \beta) = \frac{1}{\frac{1}{\text{SNR}(d_0, \alpha)} + \beta \bar{\kappa}(d_0, \Delta d, \alpha)}. \tag{34}$$

Clearly, when the jamming user is not present ($\beta = 0$) the effective SNR becomes $\text{SNR}(d_0, \alpha)$. Naturally, the achievable capacity in this situation is $C_0 \triangleq C(d_0, \alpha) = \log_2(1 + \text{SNR}(d_0, \alpha))$. On the other hand, the achievable capacity in the presence of a jamming signal with power $\beta P_T$ is

$$C(d_0, \Delta d, \alpha, \beta) = \log_2 \left( 1 + \frac{1}{\frac{1}{\text{SNR}(d_0, \alpha)} + \beta \bar{\kappa}(d_0, \Delta d, \alpha)} \right). \tag{35}$$

For a given $\beta$, it is clear that the jamming rejection can increase if the power ratio decreases. To assess the impact of the jamming signal on the legitimate link, one can define the normalized achievable capacity as

$$\bar{C}(d_0, \Delta d, \alpha, \beta) = \frac{C(d_0, \Delta d, \alpha, \beta)}{C_0}, \tag{36}$$

is the ratio between the capacity with and without the jamming signal.

Fig. 7 shows the normalized achievable capacity considering different values of $\beta$, different reference distances $d_0$ along the array's broadside ($\alpha = 0$), and a jamming user in the beamforming direction with a relative displacement $\Delta d = [0, 500\lambda]$.

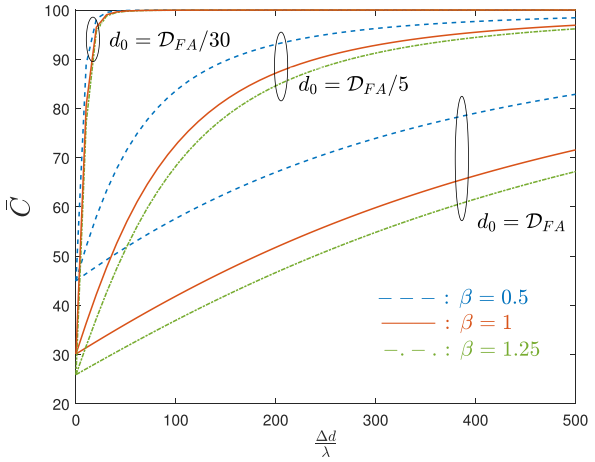


**FIGURE 7.** Normalized achievable capacity considering different values of $\beta$ and different field regions.

As can be noted from the figure, a higher value of $\beta$ increases the jamming ability. Moreover, when the legitimate user is in the far field, the achievable capacity increases slowly as the jamming user moves away (i.e., when $\Delta d$ increases), which is explained by the fact that the array does not exhibit spatial selectivity in the beamforming direction (i.e., both users experience the same array gain in this field region). In fact, in the far field, the normalized power gain is dictated by (23), confirming that the beam-focusing effect is not available. However, when the legitimate user is in the near field, the jamming effect reduces substantially when the jamming user moves away from the beamforming target at $d_0$, which is explained by the fact that the array is filtering signals in the beamforming direction ($\bar{G} < 1$). For instance, when $\beta = 1$, the normalized achievable capacity at $\Delta d = 50\lambda$ is 31%, 55% and 95% considering far-field, near-field with $d_0 = \frac{\mathcal{D}_{FA}}{5}$ and near-field with $d_0 = \frac{\mathcal{D}_{FA}}{30}$, respectively. This demonstrates that in the near field region, the array has a higher ability to filter out jamming signals.

Fig. 8 shows the evolution of the achievable capacity for different occupations ratios $O$ when the jamming user is in the beamforming direction, operates with $\beta = 1$ and can be located with a relative displacement $\Delta d = [0, 500\lambda]$. It is assumed that the legitimate user has a reference distance $d_0$ equal to the Fraunhofer array distance ($\mathcal{D}_{FA}$) for the scenario where $O = 4\%$. As a result, when $O = 4\%$, the communication occurs in the far-field.

As expected, when $O = 4\%$, the capacity decreases slowly as the jamming user moves away from the legitimate user since the focal point $d_0$ is located in the far field. As $O$ increases, the physical size of the effective ELAA sub-array increases, and the achievable capacity increases for the same

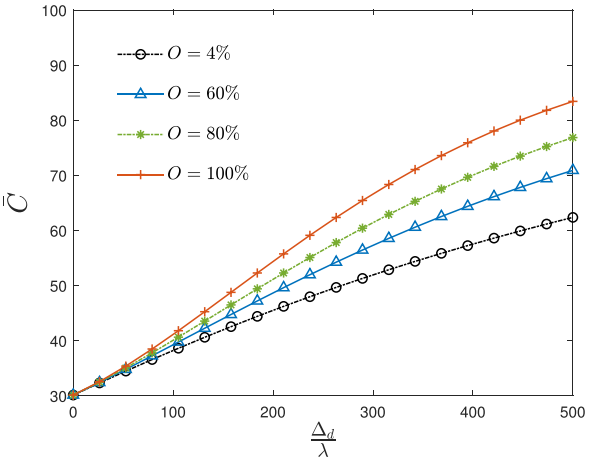


**FIGURE 8.** Normalized achievable capacity for different occupation ratios $O$.

displacement $\Delta d$. This is explained by the fact that the focal point enters the near-field, where the beam-focusing effect is available. As expected, the best performance in terms of jamming rejection happens when $O = 100\%$, where the legitimate user is located in the near-field and the beam depth is small. This means that the fraction of active antennas of the ELAA can increase or decrease according to indented level jamming rejection, which brings an additional degree of freedom to manage resources based on the required level of PLS.

## V. CONCLUSION

In this work, we studied PLS features associated with the communication with ELAAs. By using an appropriate channel model that captures the near-field effects, we presented a study of the power ratio between a legitimate and a malicious user that highlights the ability of ELAAs to spatially filter signals along a given beamforming direction. It is demonstrated that this ability depends on the field region and only exists in the near-field, where beam-focusing can be used to increase the secrecy rate and the jamming rejection features. Since the classification of the field region is dependent on the effective antenna array size, it was demonstrated that the PLS features can be controlled by modifying the number of active antennas of the ELAA, leading to an interesting degree of freedom to manage PLS in upcoming 6G communications.

Concerning future work, we consider the development of new optimized beamforming algorithms that take into account the near field particularities of non-LoS scenarios an interesting research opportunity. Another interesting direction of future work might be to use the high positioning capabilities of ELAAs to identify the position of malicious users and use that information for secure beamforming.

## REFERENCES

[1] L. Lu, G. Y. Li, A. L. Swindlehurst, A. Ashikhmin, and R. Zhang, "An overview of massive MIMO: Benefits and challenges," *IEEE J. Sel. Topics Signal Process.*, vol. 8, no. 5, pp. 742–758, Oct. 2014.

[2] M. Giordani, M. Polese, M. Mezzavilla, S. Rangan, and M. Zorzi, "Toward 6G networks: Use cases and technologies," *IEEE Commun. Mag.*, vol. 58, no. 3, pp. 55–61, Mar. 2020.

[3] R. Alghamdi, R. Alhadrami, D. Alhothali, H. Almorad, A. Faisal, S. Helal, R. Shalabi, R. Asfour, N. Hammad, A. Shams, N. Saeed, H. Dahrouj, T. Y. Al-Naffouri, and M.-S. Alouini, "Intelligent surfaces for 6G wireless networks: A survey of optimization and performance analysis techniques," *IEEE Access*, vol. 8, pp. 202795–202818, 2020.

[4] A. F. Molisch, V. V. Ratnam, S. Han, Z. Li, S. L. H. Nguyen, L. Li, and K. Haneda, "Hybrid beamforming for massive MIMO: A survey," *IEEE Commun. Mag.*, vol. 55, no. 9, pp. 134–141, Sep. 2017.

[5] X. Tian, Z. Wang, H. Li, M. Li, and Z. Sun, "Secure hybrid beamforming with low-resolution phase shifters in mmWave MIMO systems," in *Proc. IEEE Global Commun. Conf. (GLOBECOM)*, Waikoloa, HI, USA, Dec. 2019, pp. 1–6.

[6] H. Akhlaghpasand, E. Björnson, and S. M. Razavizadeh, "Jamming suppression in massive MIMO systems," *IEEE Trans. Circuits Syst. II, Exp. Briefs*, vol. 67, no. 1, pp. 182–186, Jan. 2020.

[7] V.-L. Nguyen, P.-C. Lin, B.-C. Cheng, R.-H. Hwang, and Y.-D. Lin, "Security and privacy for 6G: A survey on prospective technologies and challenges," *IEEE Commun. Surveys Tuts.*, vol. 23, no. 4, pp. 2384–2428, 4th Quart., 2021.

[8] V. Ziegler, P. Schneider, H. Viswanathan, M. Montag, S. Kanugovi, and A. Rezaki, "Security and trust in the 6G era," *IEEE Access*, vol. 9, pp. 142314–142327, 2021.

[9] L. Mucchi, S. Jayousi, S. Caputo, E. Panayirci, S. Shahabuddin, J. Bechtold, I. Morales, R.-A. Stoica, G. Abreu, and H. Haas, "Physical-layer security in 6G networks," *IEEE Open J. Commun. Soc.*, vol. 2, pp. 1901–1914, 2021.

[10] S. Hu, F. Rusek, and O. Edfors, "Beyond massive MIMO: The potential of data transmission with large intelligent surfaces," *IEEE Trans. Signal Process.*, vol. 66, no. 10, pp. 2746–2758, May 2018.

[11] E. Basar, M. Di Renzo, J. De Rosny, M. Debbah, M.-S. Alouini, and R. Zhang, "Wireless communications through reconfigurable intelligent surfaces," *IEEE Access*, vol. 7, pp. 116753–116773, 2019.

[12] E. Björnson and L. Sanguinetti, "Power scaling laws and near-field behaviors of massive MIMO and intelligent reflecting surfaces," *IEEE Open J. Commun. Soc.*, vol. 1, pp. 1306–1324, 2020.

[13] R. F. Harrington, *Time-Harmonic Electromagnetic Fields*. New York, NY, USA: McGraw-Hill, 1961, p. 110.

[14] D. Dardari, "Communicating with large intelligent surfaces: Fundamental limits and models," *IEEE J. Sel. Areas Commun.*, vol. 38, no. 11, pp. 2526–2537, Nov. 2020.

[15] H. Lu and Y. Zeng, "Communicating with extremely large-scale array/surface: Unified modeling and performance analysis," *IEEE Trans. Wireless Commun.*, vol. 21, no. 6, pp. 4039–4053, Jun. 2022.

[16] E. Björnson, Ö. T. Demir, and L. Sanguinetti, "A primer on near-field beamforming for arrays and reconfigurable intelligent surfaces," in *Proc. 55th Asilomar Conf. Signals, Syst., Comput.*, Oct. 2021, pp. 105–112.

[17] H. Zhang, N. Shlezinger, F. Guidi, D. Dardari, M. F. Imani, and Y. C. Eldar, "Beam focusing for near-field multiuser MIMO communications," *IEEE Trans. Wireless Commun.*, vol. 21, no. 9, pp. 7476–7490, Sep. 2022.

[18] Y. Han, S. Jin, M. Matthaiou, T. Q. S. Quek, and C.-K. Wen, "Towards extra large-scale MIMO: New channel properties and low-cost designs," *IEEE Internet Things J.*, vol. 10, no. 16, pp. 14569–14594, Aug. 2023.

[19] F. Oggier and B. Hassibi, "The secrecy capacity of the MIMO wiretap channel," *IEEE Trans. Inf. Theory*, vol. 57, no. 8, pp. 4961–4972, Aug. 2011.

[20] A. Mukherjee, B. Ottersten, and L.-N. Tran, "On the secrecy capacity of MIMO wiretap channels: Convex reformulation and efficient numerical methods," *IEEE Trans. Commun.*, vol. 69, no. 10, pp. 6865–6878, Oct. 2021.

[21] E. Choi, M. Oh, J. Choi, J. Park, N. Lee, and N. Al-Dhahir, "Joint precoding and artificial noise design for MU-MIMO wiretap channels," *IEEE Trans. Commun.*, vol. 71, no. 3, pp. 1564–1578, Mar. 2023.

[22] W. Alhakami, H. S. El-Sayed, O. S. Faragallah, and M. G. El-Mashed, "Efficient security architecture for physical layer in mmWave communication systems," *IEEE Access*, vol. 10, pp. 113923–113934, 2022.

[23] S. Jyothsna and L. N. Theagarajan, "Improving MIMO secrecy rate through efficient power allocation," in *Proc. IEEE 96th Veh. Technol. Conf. (VTC-Fall)*, London, U.K., Sep. 2022, pp. 1–5.

[24] D. Kapetanovic, G. Zheng, and F. Rusek, "Physical layer security for massive MIMO: An overview on passive eavesdropping and active attacks," *IEEE Commun. Mag.*, vol. 53, no. 6, pp. 21–27, Jun. 2015.
[25] G. J. Anaya-López, J. P. González-Coma, and F. J. López-Martínez, "Spatial degrees of freedom for physical layer security in XL-MIMO," in *Proc. IEEE 95th Veh. Technol. Conf. (VTC-Spring)*, Helsinki, Finland, Jun. 2022, pp. 1–5.
[26] Z. Zhang, Y. Liu, Z.-J. Wang, X. Mu, and J. Chen, "Physical layer security in near-field communications: What will be changed?" 2023, *arXiv:2302.04189*.
[27] J. Ferreira, J. Guerreiro, R. Dinis, and M. Silva, "On the jamming rejection features of near-field beamforming," in *Proc. IEEE VTC'23 (Spring)*, Jun. 2023, pp. 1–5.
[28] M. S. Neiman, "The principle of reciprocity in antenna theory," *Proc. IRE*, vol. 31, no. 12, pp. 666–671, Dec. 1943.
[29] H. T. Friis, "A note on a simple transmission formula," *Proc. IRE*, vol. 34, no. 5, pp. 254–256, May 1946.
[30] K. T. Selvan and R. Janaswamy, "Fraunhofer and Fresnel distances: Unified derivation for aperture antennas," *IEEE Antennas Propag. Mag.*, vol. 59, no. 4, pp. 12–15, Aug. 2017.
[31] A. Kay, "Near-field gain of aperture antennas," *IRE Trans. Antennas Propag.*, vol. 8, no. 6, pp. 586–593, Nov. 1960.
[32] F. Guidi and D. Dardari, "Radio positioning with EM processing of the spherical wavefront," *IEEE Trans. Wireless Commun.*, vol. 20, no. 6, pp. 3571–3586, Jun. 2021.
[33] C. E. Shannon, "A mathematical theory of communication," *Bell Syst. Tech. J.*, vol. 27, no. 3, pp. 379–423, Jul. 1948.
[34] J. Barros and M. R. D. Rodrigues, "Secrecy capacity of wireless channels," in *Proc. IEEE Int. Symp. Inf. Theory*, Jul. 2006, pp. 356–360.

**JOÃO FERREIRA** received the M.Sc. degree in electrical and computer engineering from Faculdade de Ciências e Tecnologias da Universidade Nova de Lisboa (FCT-UNL), in 2023, where he is currently pursuing the Ph.D. degree. He is also a Lecturer with FCT-UNL. His research interests include signal processing and channel modeling for wireless communications.

**JOÃO GUERREIRO** (Senior Member, IEEE) received the M.Sc. and Ph.D. degrees in electrical and computer engineering from Faculdade de Ciências e Tecnologias da Universidade Nova de Lisboa (FCT-UNL), in 2012 and 2016, respectively. He is currently an Assistant Professor with FCT-UNL. He is also a Researcher with Instituto de Telecomunicações. Since 2013, he has been actively involved in scientific research in the field of wireless communications, including signal processing, transceiver design, and channel modeling. He has published more than 30 journal articles, 60 conference papers (one best paper award), three patents (granted or pending), and two book chapters. He has participated in several national and international research projects in the last few years.

**RUI DINIS** (Senior Member, IEEE) received the Ph.D. degree from Instituto Superior Técnico (IST), Technical University of Lisbon, Portugal, in 2001, and the Habilitation degree in telecommunications from Faculdade de Ciências e Tecnologia (FCT), Universidade Nova de Lisboa (UNL), in 2010. From 2001 to 2008, he was an Assistant Professor with IST. Since 2003, he has been an Invited Researcher with Carleton University, Ottawa, Canada. He was a Researcher with Centro de Análise e Processamento de Sinal (CAPS), IST, from 1992 to 2005, and a Researcher with Instituto de Sistemas e Robótica (ISR), from 2005 to 2008. Since 2009, he has been a Senior Researcher with Instituto de Telecomunicações (IT). He is currently a Full Professor with FCT-UNL. His research interests include transmission, estimation, and detection techniques for wireless communications. He is a VTS Distinguished Speaker and a ComSoc Distinguished Lecturer. He is or was an Editor of IEEE TRANSACTIONS ON WIRELESS COMMUNICATIONS, IEEE TRANSACTIONS ON COMMUNICATIONS, IEEE TRANSACTIONS ON VEHICULAR TECHNOLOGY, IEEE OPEN JOURNAL OF THE COMMUNICATIONS SOCIETY, and *Physical Communication* (Elsevier). He was a guest editor for several special issues.